Analysis of Vertical GaN JBS and p-n Diodes by Mg Ion Implantation and Ultrahigh-Pressure Annealing

Shane R. Stein, Dolar Khachariya, Will Mecouch, Seiji Mita, Pramod Reddy, James Tweedie, Kacper Sierakowski, Grzegorz Kamler, Michal Bockowski, Erhard Kohn, *Life Member, IEEE*, Zlatko Sitar, Ramón Collazo, and Spyridon Pavlidis, *Member, IEEE*

***Abstract*— We report on vertical GaN junction barrier Schottky (JBS) diodes formed by Mg ion implantation and ultrahigh -pressure annealing (UHPA). The static ON-state characteristics of the diodes show an ideality factor of 1.05, a turn-on voltage of ∼0.7 V, a current rectification ratio of $\sim 10^{11}$, and a low differential specific ON-resistance that scales with Schottky stripe width in fair agreement with the analytical model. The reverse leakage dependence on Schottky stripe width also agrees well with the analytical model. Implanted p-n junction diodes fabricated on the same wafer exhibit avalanche breakdown in reverse bias with a positive temperature coefficient, but the forward current is limited by a series barrier. Temperature-dependent current–voltage measurements of th p-n diodes verify the presence of the implanted p-n junction and reveal an additional 0.43-eV barrier, which we hypothesize arises from a p-Schottky contact and forms a second diode back-to-back with the p-n junction. This interpretation is supported by analysis of the capacitance–voltage characteristics of the implanted p-n diodes, epitaxial p-n diodes fabricated with intentional p-Schottky contacts, and comparison to TCAD simulations. Ultimately, the presence of the p-Schottky contact does not hinder JBS diode operation. The use of diffusion-aware designs and/or diffusion reduction represents future directions for Mg implantation technology in GaN power devices.**

***Index Terms*— Ion implantation, junction barrier Schottky (JBS) diode, Mg activation, p-n diode, power semiconductor device, Schottky contact, ultrahigh-pressure annealing (UHPA), vertical GaN.**

Manuscript received 9 October 2023; revised 21 November 2023; accepted 22 November 2023. This work was supported in part by the U.S. Department of Energy's Advanced Research Projects Agency-Energy (ARPA-E) through Power Nitride Doping Innovation Offers Devices Enabling SWITCHES (PNDIODES) Program, under Grant DE-AR0000873 and Grant DE-AR0001492; in part by North Carolina State University Faculty Start-up Fund; in part by the National Science Foundation under Grant ECCS-1916800, Grant ECCS-1508854, Grant ECCS-1610992, Grant DMR-1508191, Grant ECCS-1653383, and Grant ECCS-2145340; in part by the Office of Naval Research Global's Naval International Cooperative Opportunities in Science and Technology Program under Grant N62909-17-1-2004; and in part by Poland's National Center for Research and Development (NCBR) under Grant TECHMATSTRATEG-III/0003/2019-00. The review of this article was arranged by Editor M. Buffolo. *(Corresponding author: Spyridon Pavlidis.)*

Shane R. Stein was with the Department of Electrical and Computer Engineering, North Carolina State University, Raleigh, NC 27695 USA. He is now with Wolfspeed, Inc., Durham, NC 27703 USA.

Dolar Khachariya, Will Mecouch, Seiji Mita, and Pramod Reddy are with Adroit Materials, Inc., Cary, NC 27539 USA.

James Tweedie was with Adroit Materials, Inc., Cary, NC 27539 USA. He is now with Wolfspeed, Inc., Durham, NC 27703 USA.

Kacper Sierakowski, Grzegorz Kamler, and Michal Bockowski are with the Institute of High-Pressure Physics, Polish Academy of Sciences, 01-142 Warsaw, Poland.

Erhard Kohn and Ramón Collazo are with the Department of Material Science and Engineering, North Carolina State University, Raleigh, NC 27695 USA.

Zlatko Sitar is with Adroit Materials, Inc., Cary, NC 27539 USA, and also with the Department of Material Science and Engineering, North Carolina State University, Raleigh, NC 27695 USA.

Spyridon Pavlidis is with the Department of Electrical and Computer Engineering, North Carolina State University, Raleigh, NC 27695 USA (e-mail: spavidis@ncsu.edu).

Color versions of one or more figures in this article are available at https://doi.org/10.1109/TED.2023.3339592.

Digital Object Identifier 10.1109/TED.2023.3339592

I. Introduction

VERTICAL GaN power devices are promising candidates for future kV-class power electronics due to the wide bandgap (WBG) and high critical electric field (E_C) of GaN [1], [2]. Many reports of high-performance vertical GaN power diodes and transistors have been published showing high breakdown voltage (BV) and low specific ON-resistance (R_{ON}) approaching the material limits [3], [4], [5], [6], aided by the availability and ongoing development of high-quality bulk GaN substrates [7].

Junction barrier Schottky (JBS) diodes are attractive candidates for WBG semiconductor power rectifiers as they combine the advantages of p-n and Schottky barrier diodes (SBDs). Unipolar SBDs possess low turn-on voltage (V_{ON}) determined by the Schottky barrier height as well as low switching losses due to the lack of reverse recovery. However, due to the high E_C of WBG semiconductors, the high electric field (E-field) at the metal–semiconductor interface in reverse bias leads to high leakage current and reduced BV due to Schottky barrier lowering and electron tunneling [8]. The lateral p-n junction grid of JBS diodes depletes and pinches off the n-type channel when blocking, in turn shielding the Schottky interface by reducing the E-field at the surface, which lowers the leakage current and enables p-n junction-limited blocking characteristics, including high BV and avalanche capability. For this reason, JBS diodes are the device of choice for commercial SiC power rectifiers [8], [9].

To form the lateral p-n junctions needed for JBS diodes as well as other power devices, such as MOSFETs or JFETs, selective area doping is required. Methods to selectively dope GaN have included etch-and-regrowth [10], [11], [12], [13] and ion implantation [14], [15], [16], [17], [18]. Etch-and-regrowth typically results in impurity-related leakage at the regrown interface, increases fabrication complexity, and makes control of the dopant profile challenging [12], [13]. Ion implantation is the standard technique for Si and SiC since it grants excellent control of the dopant profile and concentration, and simplifies device design and fabrication. Yet, the activation of implanted ions in GaN has long been hindered by the tendency of the GaN surface to decompose at high temperatures [19]. Various specialized postimplantation annealing techniques have been studied, but challenges with damage removal and activation remain [14], [15], [16], [17], [18]. It has also been observed that capping layers do not fully prevent decomposition and are difficult to strip following the anneal [20]. Recently, ultrahigh-pressure annealing (UHPA), wherein sufficiently high N_2 overpressure is used to stabilize the GaN surface during the high-temperature anneal, has routinely provided high-implanted Mg activation ratios of ~70%–100% after annealing at 1300 °C–1400 °C, without the need for a capping layer [21], [22], [23], [24].

Recently, vertical GaN JBS diodes have been reported using Mg ion implantation followed by UHPA [25], [26], demonstrating high BV and low differential R_{ON}. This work is a continuation of our previous work on JBS diodes formed by Mg ion implantation and subsequent UHPA [25] and characterizes the forward and reverse current–voltage (I–V) characteristics, as well as the dependence on the JBS stripe width (w_n), and compares them with the theoretical model [8]. In addition, we discuss the temperature-dependent forward and reverse bias I–V characteristics of p-n junction diode test structures fabricated on the same wafer to isolate the behavior of the implanted junctions and p-contacts. These diodes exhibit avalanche capability, which, to the best of authors' knowledge, is the first such report for GaN p-n diodes formed via Mg implantation and UHPA. The capacitance–voltage (C–V) characteristics of the p-n diodes are compared to simulation to understand the role of the p-contact. Overall, it is found that the electrical behavior of the devices is dominated by the p-contact and Mg diffusion, rather than by defects resulting from implantation or annealing. These results help inform design rules for future work.

II. Device Fabrication and Layout

Schematic cross sections of the fabricated JBS and p-n diodes on the same wafer are shown in Fig. 1(a) and (b), respectively. First, a 5-μm-thick n-GaN drift layer was grown on a 2-in, 370-μm-thick conductive ammonothermal GaN substrate using a vertical, cold-wall, radio frequency-heated, low-pressure metal-organic chemical vapor deposition (MOCVD) reactor using chemical potential control and defect quasi-Fermi level control [27]. These techniques reduce carbon compensation in the film, allowing controllable Si-doping at the low concentrations necessary to obtain a high blocking voltage in conjunction with high electron mobility for minimizing ON-state resistance. The selective p-type regions were obtained by room-temperature (RT) Mg ion implantation, with a tilt angle of 7°, using two ion energies of 25 and 75 keV with corresponding doses of 4.4×10^{13} and 2×10^{14} cm^{-2}, respectively, to form a ~100-nm-deep box profile with a Mg concentration of $\sim 2 \times 10^{19}$ cm^{-3}. After stripping the implantation mask, damage recovery and dopant activation were achieved via UHPA at 1300 °C for 30 min at a pressure of 400 MPa in N_2 ambient. Based on [21], this annealing condition is expected to give a high activation ratio ≥80%, a peak Mg concentration of $\sim 2 \times 10^{18}$ cm^{-3}, and a deep Mg diffusion tail with a final metallurgical junction depth (t_p) of ~2 μm. Fig. 1(c) shows a schematic visualization of the implanted Mg depth profile before and after UHPA.

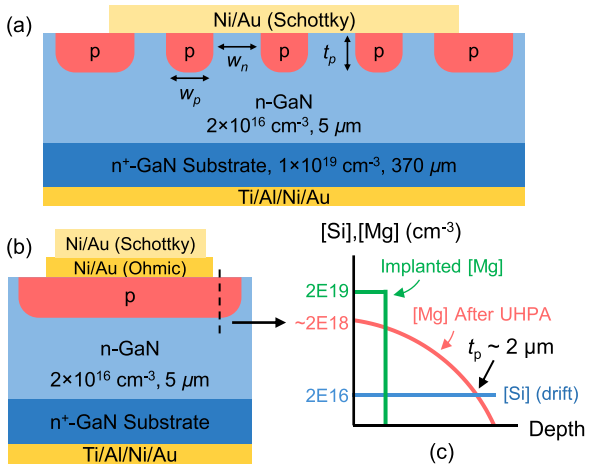

Fig. 1. Schematic cross section of the fabricated: (a) JBS diode and (b) p-n diode. (c) Schematic representation of the implanted Mg depth profile along the cutline in (b) before and after UHPA.

Following UHPA, the surface was treated to obtain near-ideal, homogeneous n-GaN Schottky contacts after UHPA [28]. Subsequently, rapid thermal annealing (RTA) at 700 °C for 10 min in the air was used to drive out any hydrogen incorporated during UHPA [29], [30]. The surface was then cleaned in 1:1 HCl:H_2O, prior to depositing Ni/Au p-type contacts by electron-beam evaporation and annealing at 600 °C for 10 min in air. Ni/Au Schottky contacts were then deposited without a subsequent contact anneal. Lastly, a large-area Ti/Al/Ni/Au n-type ohmic contact was evaporated onto the backside of the substrate for the cathode.

A linear stripe cell geometry is used for the JBS diodes with variable Schottky n-stripe width (w_n) ranging from 2 to 8 μm and p-stripe width (w_p) of 4 μm. Only JBS diodes with the unannealed Ni/Au Schottky metal are discussed in this study [Fig. 1(a)]. JBS diodes that also included the annealed Ni/Au contacts on the p-GaN stripes were fabricated as well, but the I–V characteristics show no difference from those without annealed contacts. An explanation for this is provided in Section IV. The anode for the p-n diodes consists of the annealed contact first with the Schottky contact on top [Fig. 1(b)]. SBDs were also fabricated on-wafer using the unannealed Ni/Au contacts. The JBS, p-n, and SBDs all have

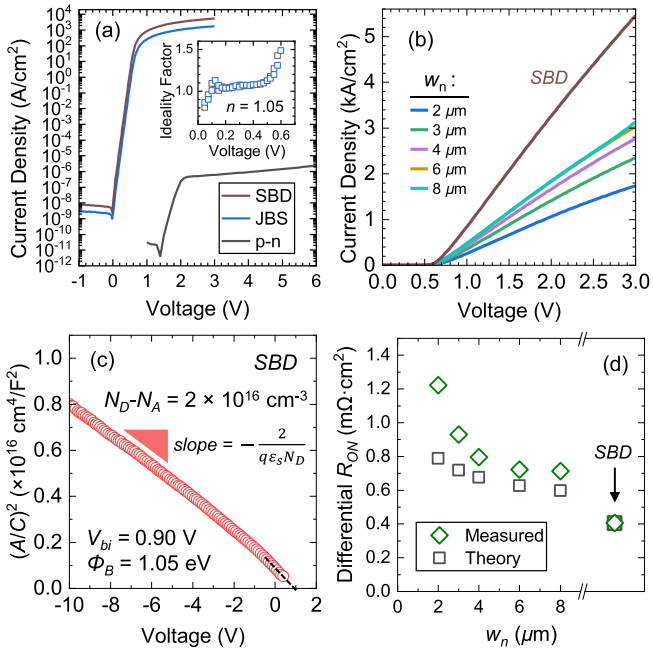

Fig. 2. (a) Semilogarithmic plot of the forward I–V characteristics of the SBD, p-n diode, and JBS diode with $w_n = 2$ μm. The extracted ideality factors are plotted against voltage in the inset. (b) Linear scale plot of the forward I–V characteristics of the SBD and JBS diodes. (c) Square of the inverse capacitance plotted versus voltage for the SBD, used to extract N_D and Φ_B. (d) Extracted differential R_{ON} for each value of w_n for the measured JBS diodes and the theoretical values.

a simple junction termination extension (JTE) formed by the Mg implantation and UHPA steps, which extend 15 μm past the edge of the anode contact. The active area of the diodes is 0.1×0.1 mm^2. For the JBS and SBD, this corresponds to the area of the Schottky contact enclosed by the JTE where carrier injection occurs, whereas for the p-n diode, it corresponds to the total p-n junction area including the JTE.

III. JBS Diode Characterization

The forward I–V characteristics of the JBS diodes and SBD in semilogarithmic and linear scales are shown in Fig. 2(a) and (b), respectively. The forward I–V of the p-n diode is also shown in Fig. 2(a) for comparison, but the analysis thereof is contained in Section IV. The data were measured using a Keithley 4200A-SCS parameter analyzer. The SBD and JBS diodes exhibit an ideality factor (n) of 1.05, indicating near-ideal Schottky characteristics dominated by thermionic emission. The diodes exhibit a high current rectification ratio of 2×10^{11}, and a turn-on voltage (V_{ON}) of ~0.65–0.7 V by linear extrapolation. C–V measurement of the SBD, shown in Fig. 2(c), reveals a net drift layer donor concentration ($N_D - N_A$) of 2×10^{16} cm^{-3} from the slope of the $(A/C)^2$–V curve. Linearly extrapolating the curve to $(A/C)^2 = 0$ yields a built-in potential (V_{bi}) of 0.90 V, from which the Schottky barrier height (ϕ_B) can be calculated as $\phi_B = qV_{bi} + (E_C - E_F) + kT = 1.05$ eV, where E_C–E_F is the difference between the conduction band edge and Fermi level and is calculated from the extracted net donor concentration. These parameters are in agreement with our previous results on Ni Schottky contacts on UHPA n-GaN [28].

The diodes also show high current density and low differential R_{ON} which varies with w_n. The analytical model [8] takes into account three regions of current flow in the JBS unit cell in forward bias. First, current flows vertically through the un-depleted portion of the n-GaN stripe of uniform width $w_n - w_d$, where w_d is the depletion width extending into the n-GaN region until it reaches the bottom of the depletion region at a depth of $t_p + w_d$. The specific resistance of this region is given by

$$R_{D1} = \frac{\rho_n (w_n + w_p)(t_p + w_d)}{(w_n - 2w_d)} \quad (1)$$

where ρ_n is the resistivity of the n-GaN given by $1/(qN_D\mu_n)$, where q is the electron charge and μ_n is the electron mobility. The current then spreads at a ~45° angle until it reaches the width of the cell and overlaps the adjacent cell current. The specific resistance of this portion is

$$R_{D2} = \frac{1}{2}\rho_n (w_n + w_p) \ln\left[\frac{(w_n + w_p)}{(w_n - 2w_d)}\right]. \quad (2)$$

From this point, the current flows in a uniform area through the remainder of the drift region with a specific resistance given by

$$R_{D3} = \rho_n \left(t_n - \frac{w_p}{2} - 2w_d\right) \quad (3)$$

where t_n is the thickness of the drift layer underneath the p-region and is equal to 3 μm. The total differential R_{ON} is calculated from the sum of the three resistance components and the substrate resistance, equal to 0.22 mΩ·cm^2 [25], and plotted as a function of w_n in Fig. 2(d) alongside the measured values. It should be noted that the analytical model does not account for Mg diffusion. An excellent fit for the SBD is obtained using $N_D = 2 \times 10^{16}$ cm^{-3}, as extracted from the C–V data, and $\mu_n = 850$ cm^2/V·s. The measured R_{ON} values of the JBS diodes are also in good agreement with the theoretical values but deviate more for smaller w_n. This is likely due to lateral Mg diffusion in the fabricated devices, which will result in larger w_p and smaller w_n compared to the nominal values, as well as possible background compensation due to the Mg diffusion tail extending beyond the p-n junction which would reduce the N_D within the JBS channel and raise the resistance [2]. Further reduction of R_{ON} for future diodes can be achieved by decreasing w_p or optimizing the annealing conditions to minimize diffusion.

Fig. 3(a) shows the reverse I–V characteristics of the JBS diodes measured using a Keithley 2657A high power source meter, overlaid with the theoretical I–V curves as well as the measured curves of the SBD and p-n diode. Note that the current measurement limit for the JBS diodes and SBD with the high voltage setup was 10^{-10} A, corresponding to a current density of 10^{-6} A. The lower current measured for the p-n diode was enabled using a smaller voltage step size to improve the current measurement resolution. The leakage current decreases as w_n becomes smaller due to the depletion of the n-GaN channel that reduces the E-field at the Schottky interface, resulting in a higher BV. The measured I–V curves of both the p-n and JBS diodes are repeatable and show no

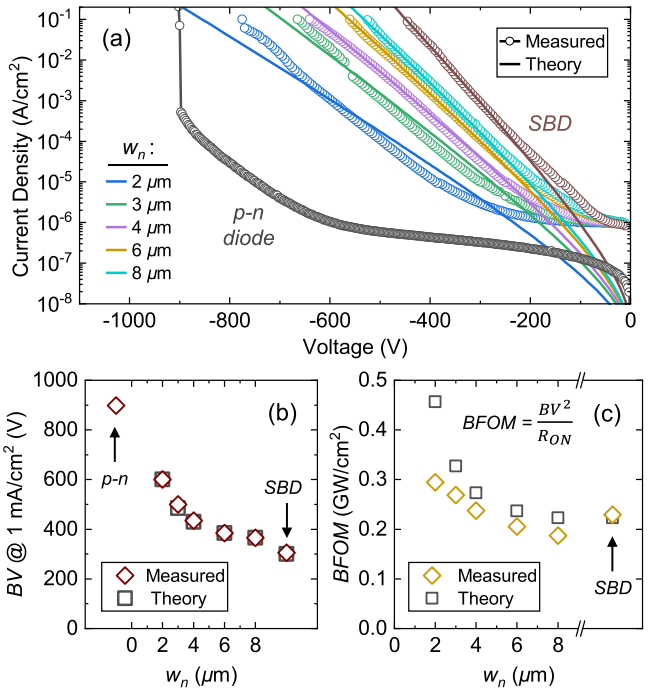

Fig. 3. (a) Reverse blocking *I–V* characteristics of the SBD, p-n, and JBS diodes for each w_n overlaid with the theoretically calculated JBS leakage current. (b) BV extracted at 1 mA/cm^2 and (c) BFOM for the diodes as a function of w_n.

destruction up to a compliance 0.1 A/cm^2. The JBS diodes do not exhibit a sharp breakdown, while the p-n diode exhibits a sharp breakdown at a BV of ~900 V.

The theoretical JBS leakage current is given by [8]

$$I_L = \left(\frac{w_n}{w_n + w_p}\right) A_R T^2 \exp\left(-\frac{q\phi_B}{kT}\right) \cdot \exp\left(\frac{q\Delta\phi_B}{kT}\right) \exp\left(C_T E_m^2\right) \quad (4)$$

where A_R is the Richardson constant for GaN and is equal to 26.4 A·K^{-2}·cm^{-2}, T is the temperature, k is Boltzmann's constant, $\Delta\phi_B$ is the change in Schottky barrier height due to image force barrier lowering, C_T is a Schottky tunneling coefficient, and E_m is the E-field at the Schottky interface. $\Delta\phi_B$ is given by

$$\Delta\phi_B = \sqrt{\frac{qE_m}{4\pi\varepsilon_s}} \quad (5)$$

where ε_s is the permittivity of GaN, and E_m is given by

$$E_m = \sqrt{\frac{2qN_D}{\varepsilon_s}(\alpha V_R + V_B)} \quad (6)$$

where V_B is the Schottky contact potential, V_R is the applied reverse voltage, and α is a coefficient used to account for the reduction of E_m due to the shielding of the Schottky contact, which for SiC has been related to the JBS aspect ratio [31] by

$$\alpha = \exp\left(-\beta\frac{t_p}{w_n}\right). \quad (7)$$

The theoretical reverse leakage current (I_L) plotted in Fig. 3(a) was calculated and fit to the experimental data using ϕ_B = 0.93 eV, $C_T = 3.62 \times 10^{-12}$ cm^2/V^2, and $\beta = 0.57$. Our C_T is two times smaller than the value obtained by Ozbek and Baliga [32] and 28 times smaller than the value obtained by Matys et al. [26], indicating that the tunneling rates of our Schottky contacts are lower than other reported values. The smaller β estimated in our devices compared to the value found for SiC (5.75 [31]) indicates a weaker shielding of the Schottky contact for our diodes. This is likely attributable to the Mg diffusion in GaN during UHPA, which grades the p-n junction [2], whereas SiC retains its abrupt junctions after activation annealing due to negligible dopant diffusion.

The BV of the JBS diodes defined by I_L = 1 mA/cm^2 for each w_n is plotted in Fig. 3(b). The measured BV increases with decreasing w_n and follows the model well. Since the R_{ON} also increases with decreasing w_n, the Baliga figure of merit (BFOM), given by BV^2/R_{ON}, is plotted in Fig. 3(c) to assess the tradeoff between BV and R_{ON} as a function of w_n. The BFOM increases with decreasing w_n across the entire range. $w_n = 2$ μm gives the highest BFOM of 0.29 GW/cm^2. Note that if a higher I_L of 0.1 A/cm^2 is used to define the BV, the BV for this diode becomes 775 V and the BFOM becomes 0.49 GW/cm^2. By improving β via optimization of the JBS aspect ratio or Mg concentration, the E-field at the Schottky contact and the resulting JBS leakage can be reduced. This would, in turn, increase the BV and BFOM of the JBS diodes until limited by junction breakdown. This requires adjusting the implantation profile or optimizing the annealing conditions to reduce the Mg diffusion.

IV. P-N Diode and Contact Characterization

In this section, the implanted p-n junctions and p-contacts are studied by characterizing p-n diode test structures fabricated on the same wafer. The reverse *I–V* breakdown curves of the p-n diode from RT to 125 °C are plotted in Fig. 4. The BV linearly increases with temperature according to the relationship $BV = BV_{RT}(1 + \gamma\Delta T)$, where γ is the temperature coefficient, which is indicative of impact ionization. Furthermore, the γ measured here is 5.5×10^{-4} K^{-1}, which is 8% smaller than the value of 6×10^{-4} K^{-1} measured for epitaxial p-n diodes [33]. This demonstration of avalanche breakdown for ion-implanted GaN p-n junctions suggests great promise for the use of UHPA for GaN power diodes and transistors requiring selective area doping, as avalanche ruggedness is important for power switching. It also indicates that, although the fabricated JBS diodes do not show a positive temperature coefficient, the same p-n junction of the JBS diodes is capable of avalanche breakdown. Therefore, if the JBS leakage can be reduced, GaN JBS diodes with avalanche capability should be demonstrable.

The temperature-dependent forward *I–V* characteristics of the p-n diode are shown in Fig. 5(a). Two different regions are noticeable: 1) below ~2 V, when the forward current is low, the current increases exponentially with an ideality factor of n = 1.95 at RT. n slightly increases with temperature up to ~2.4 at 80 °C and 2) above ~2 V, the current abruptly becomes limited at a forward current of ~10^{-6} A/cm^2,

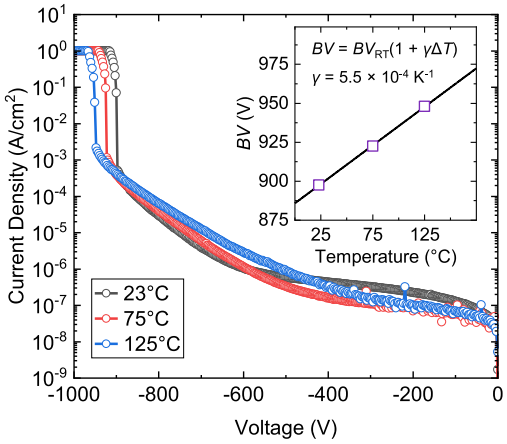

Fig. 4. Reverse breakdown curves for the p-n diode from RT to 125 °C. Inset shows the BV versus temperature, demonstrating a positive temperature coefficient which indicates avalanche breakdown.

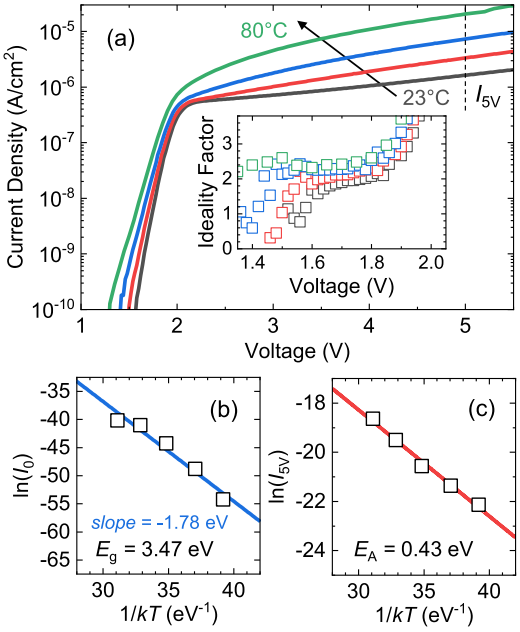

Fig. 5. (a) Forward I–V characteristics of the implanted p-n diode from RT to 80 °C. The inset shows the ideality factor of the diode in the exponential region for each temperature. (b) Plot of $\ln(I_0)$ versus $1/kT$ for the p-n diode, used to extract the bandgap of GaN from the junction current. (c) Arrhenius plot of the current taken at 5 V, which gives an estimated energy barrier of 0.43 eV for the current limiter.

showing a weak voltage dependence but strong temperature dependence. The n of 1.95 at RT suggests that the conduction mechanism at low current is a mixture of diffusion current and Shockley–Read–Hall recombination current at the p-n junction. The change of conduction mechanism at ~2 V points to a current-limiting mechanism in series with the p-n junction, so that once the junction becomes more conductive (above $\sim 10^{-6}$ A/cm^2), the second mechanism takes over.

The presence of the GaN p-n junction can be verified by the temperature dependence of the exponential region of the I–V. The temperature dependence of the saturation current (I_0) of

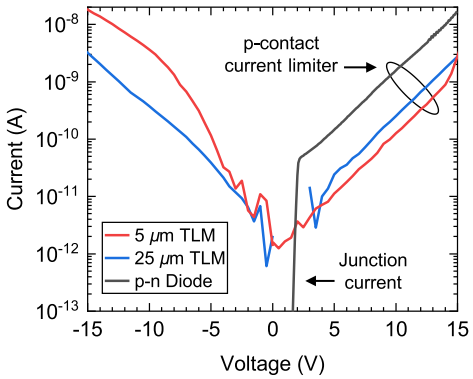

Fig. 6. Forward I–V characteristics of the implanted p-n diode and I–V characteristics of TLM structures fabricated using the same anode contact scheme for two different contact spacings.

a p-n junction is approximately [34]

$$I_0 \propto \exp\left(-qE_g/nkT\right) \tag{8}$$

where E_g is the bandgap of the semiconductor. I_0 for the p-n diode is linearly extrapolated from the exponential region of the I–V, and $\ln(I_0)$ is plotted against $1/kT$ in Fig. 5(b). The slope of this relationship is $-E_g/n = -1.78$. Therefore, E_g for the p-n junction can be estimated from the temperature-dependent I–V by multiplying the slope by the value of n at RT. The extracted value of E_g is 3.47 eV, which is very close to the E_g of GaN and confirms that the exponential portion of the forward I–V is due to the GaN p-n junction.

The temperature dependence of the series current-limiting mechanism is also analyzed via an Arrhenius plot of $\ln(I)$ taken at 5 V versus $1/kT$, as shown in Fig. 5(c). The slope gives an activation energy (E_A) of 0.43 eV. This value is close to the Schottky barrier height measured for unannealed Ni contacts on highly doped epitaxial p-GaN [35]. It is known that the Mg concentration at the GaN surface is reduced to $\sim 2 \times 10^{18}$ cm^{-3} after UHPA due to drive-in [21], which would be expected to result in a significant barrier height even with contact annealing. Therefore, the Ni/Au contact likely forms a p-Schottky diode back-to-back with the p-n junction, so that when the p-n diode is forward-biased, the reverse-biased p-Schottky diode limits the current to $\sim 10^{-6}$ A/cm^2 based on the reverse Schottky leakage level.

Fig. 6 shows the forward I–V of the implanted p-n diode at RT up to 15 V overlaid with I–V curves of rectangular transfer length method (TLM) test structures with contact spacings of 5 and 25 μm fabricated using the same anode contact scheme as the p-n diode. The TLM current is highly non-ohmic, exhibits the same exponential slope as the p-n diode in the current-limited region, and shows no dependence on lateral contact spacing. These characteristics further support the hypothesis that the p-n diode current is limited by the anode contact rather than bulk effects.

To investigate this hypothesis, the C–V characteristics of the p-n diode were studied. Fig. 7(a) shows the measured C–V of the implanted p-n diode, as well as the simulated C–V of the device using Silvaco TCAD, taking into account the p-Schottky contact and the diffused acceptor profile. Both

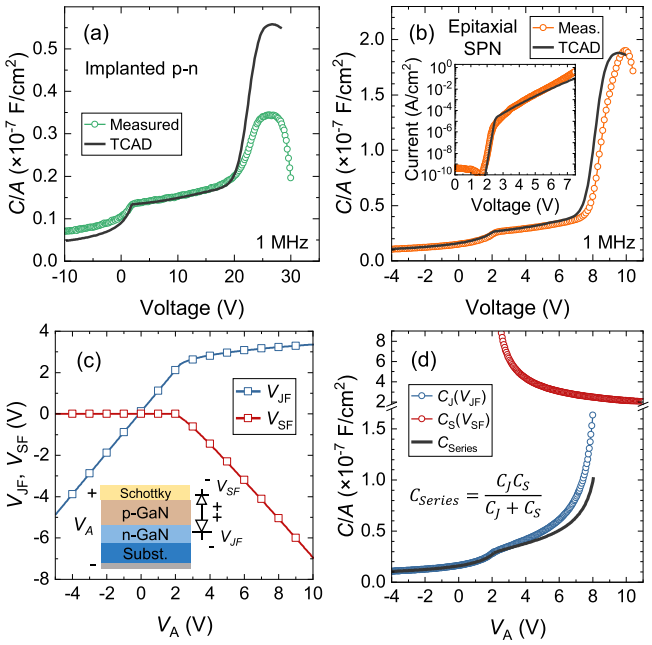

Fig. 7. Measured and simulated C–V characteristics of: (a) implanted p-n diode and (b) epitaxial p-n diode with Ni/Au Schottky p-contact, with inset showing the forward I–V of the device. (c) Dependence of the forward voltage drop across the p-n junction and p-Schottky contact on the total applied voltage. (d) Theoretical depletion capacitance of each diode and the series capacitance plotted against the total applied voltage while taking into account the voltage division between the back-to-back diodes.

curves give unique C–V characteristics, consisting of two different regions separated by a kink, similar to the I–V. At low voltages, the capacitance exhibits a typical $(V_R)^{-1/2}$ dependence of a depletion capacitance. At ~2 V, the same voltage where the series barrier begins to limit the forward current, the slope of the C–V curve abruptly decreases, until the capacitance eventually rises again to a peak at ~25 V before turning over with a negative slope. The poor overlap below ~2 V and above ~20 V points to imperfections in the model. To address these, future studies will focus on more precisely modeling the doping profiles near the junction and considering the impact of defects.

To further assist with the C–V analysis and verify the role of the Schottky p-contact, epitaxial p-n diodes were fabricated with unannealed Ni/Au anodes, to allow a direct analysis of a Schottky-p-n (SPN) structure with abrupt junctions and uniform doping profiles. The epitaxial stack from top to bottom consisted of 300 nm of 2×10^{19} cm^{-3} Mg-doped p-GaN followed by 5 μm of ~10^{16} cm^{-3} Si-doped n-GaN, on top of a conductive ammonothermal n-GaN substrate. The measured and simulated I–V and C–V characteristics of this device are shown in Fig. 7(b). The measured and simulated data match well, and very similar characteristics as the implanted diode are observed but over a narrower voltage range, likely due to the higher Mg concentration of 2×10^{19} cm^{-3}. The excellent overlap can be attributed to better agreement between the experimental and simulated structures with an abrupt junction and uniform doping profiles. It is also worth noting that when performing the same temperature dependent I–V analysis as

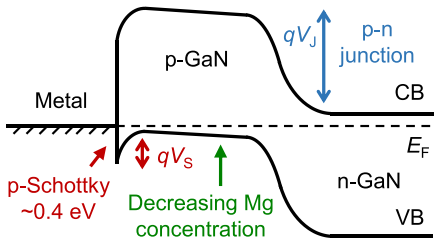

Fig. 8. Proposed energy band diagram of the implanted vertical GaN p-n diode, consisting of a p-n junction in series with a p-Schottky contact, and a decreasing Mg concentration toward the p-n junction.

illustrated in Fig. 6 for the SPN diode (not shown), an E_g of 3.71 eV and E_A of 0.33 eV are extracted, validating this technique for the estimation of the GaN bandgap and giving a similar value for the p-Schottky barrier height.

The C–V characteristics of the SPN can be explained by a division of the total applied voltage (V_A) between the two back-to-back diodes. Fig. 7(c) shows the forward voltage drop across the Schottky contact (V_{SF}) and across the p-n junction (V_{JF}) as a function of V_A, which were extracted from the device band diagram at each bias point using the TCAD simulation. At low voltages, when the Schottky contact is forward-biased or the total current is below the leakage level of the Schottky contact, V_{SF} is zero and independent of V_A. Thus, in this voltage range, all of the applied voltage is dropped across the p-n junction and the I–V and C–V characteristics are solely determined by the junction. Once the Schottky contact begins to limit the current at higher voltages, the rate at which V_{JF} increases with V_A abruptly decreases and most of the additional voltage is dropped across the reverse-biased Schottky contact. Thus, the C–V curve of the p-n junction in this region appears stretched out with respect to V_A, until V_{JF} eventually reaches the junction built-in potential at a much higher value of V_A and the junction capacitance finally approaches infinity. The turnover in capacitance after this point is due to the high leakage current of the Schottky contact at sufficiently high voltage. Using the known dependence of V_{SF} and V_{JF} on V_A, the theoretical depletion capacitances of the two diodes (C_S, C_J) and the total series capacitance were plotted against V_A in Fig. 7(d). The theoretical series capacitance of the back-to-back diodes with proper accounting of the voltage division between them successfully replicates the kink and change of slope observed for the measured and simulated C–V of the epitaxial and implanted p-n diodes, further supporting the SPN model.

The equilibrium energy band diagram of the proposed SPN model for the implanted p-n diode is shown in Fig. 8. The key components include the nonabrupt p-n junction at a depth t_p from the surface determined by the diffusion of the implanted Mg during UHPA, and the p-Schottky diode at the surface which results from the low-surface Mg concentration after diffusion. As the Mg concentration decreases across the diffusion tail toward the junction, the Fermi level (E_F) gradually moves farther from the valence band (VB).

The Schottky-like behavior of the p-contact indicates that the contact annealing procedure that was used cannot currently produce ohmic contacts to the p-GaN, perhaps due to insufficient Mg concentration at the GaN surface due to UHPA-induced diffusion. Yet, since V_{SF} remains equal to 0 V and V_A is dropped entirely across the p-n junction when the diode is reverse-biased, as shown in Fig. 7(c), the p-contact can directly modulate the junction to deplete the n-type channel of the JBS diode in reverse bias without being ohmic. Therefore, the Schottky-like p-contacts are sufficient for obtaining excellent JBS diode operation, as well as avalanche breakdown for p-n junctions. This also explains why JBS diodes with annealed and unannealed p-contacts show identical I–V characteristics, as mentioned in Section II. For other devices, such as merged pin-Schottky (MPS) diodes requiring surge capability or power MOSFETs with a flyback body diode for which bipolar carrier injection at the p-n junction is needed, an ohmic p-contact will be required. An investigation of different contact annealing conditions to obtain ohmic contacts to p-GaN with lower Mg concentration and/or p-GaN formed by ion implantation and UHPA will be worthwhile for these applications. Alternatively, the use of regrown p-GaN contact layers with high Mg concentration on Mg-implanted regions could be used. In the former approach, optimization of the implantation or annealing conditions to account for or minimize Mg drive-in would also facilitate the formation of ohmic contacts, while improving the R_{ON} and BV of JBS diodes as well.

V. Conclusion

In conclusion, JBS diodes were demonstrated with excellent static ON-state characteristics, namely, ON-resistance and reverse leakage current that scale with the Schottky stripe width in agreement with the analytical model. Moreover, the implanted p-n junctions exhibit an RT BV of ∼900 V and avalanche capability characterized by a positive BV temperature coefficient. Temperature-dependent I–V and C–V measurements reveal that the forward current of the p-n diodes is limited by the contact with the implanted p-GaN, which forms a reverse-biased Schottky diode back-to-back with the forward-biased p-n junction, possibly due to Mg diffusion away from the surface. While an impediment to forward surge capability, this does not prevent the implanted p-GaN grid under the anode from screening the Schottky interface and reducing leakage current. These results underline the promise of UHPA for GaN power devices requiring selective area doping.

References

[1] J. A. Cooper and D. T. Morisette, "Performance limits of vertical unipolar power devices in GaN and 4H-SiC," *IEEE Electron Device Lett.*, vol. 41, no. 6, pp. 892–895, Jun. 2020, doi: 10.1109/LED.2020.2987282.

[2] S. R. Stein, D. Khachariya, and S. Pavlidis, "Design and performance analysis of GaN vertical JFETs with ion-implanted gates," *Semiconductor Sci. Technol.*, vol. 37, no. 12, Nov. 2022, Art. no. 125011, doi: 10.1088/1361-6641/ac9d00.

[3] L. Yates et al., "Demonstration of >6.0-kV breakdown voltage in large area vertical GaN p-n diodes with step-etched junction termination extensions," *IEEE Trans. Electron Devices*, vol. 69, no. 4, pp. 1931–1937, Apr. 2022, doi: 10.1109/TED.2022.3154665.

[4] Y. Saitoh et al., "Extremely low on-resistance and high breakdown voltage observed in vertical GaN Schottky barrier diodes with high-mobility drift layers on low-dislocation-density GaN substrates," *Appl. Phys. Exp.*, vol. 3, no. 8, Jul. 2010, Art. no. 081001, doi: 10.1143/apex.3.081001.

[5] T. Oka, T. Ina, Y. Ueno, and J. Nishii, "1.8 mΩ·cm^2 vertical GaN-based trench metal–oxide–semiconductor field-effect transistors on a free-standing GaN substrate for 1.2-kV-class operation," *Appl. Phys. Exp.*, vol. 8, no. 5, May 2015, Art. no. 054101, doi: 10.7567/apex.8.054101.

[6] J. Liu et al., "1.2 kV vertical GaN fin JFETs with robust avalanche and fast switching capabilities," in *IEDM Tech. Dig.*, Dec. 2020, pp. 23.2.1–23.2.4, doi: 10.1109/IEDM13553.2020.9372048.

[7] R. Kucharski, T. Sochacki, B. Lucznik, and M. Bockowski, "Growth of bulk GaN crystals," *J. Appl. Phys.*, vol. 128, no. 5, Aug. 2020, Art. no. 050902, doi: 10.1063/5.0009900.

[8] B. J. Baliga, *Gallium Nitride and Silicon Carbide Power Devices*. Hackensack, NJ, USA: World Scientific, 2016.

[9] *Discrete Silicon Carbide Schottky Diodes*. Wolfspeed. Accessed: Mar. 14, 2023. [Online]. Available: https://www.wolfspeed.com/products/power/sic-schottky-diodes/

[10] A. T. Binder et al., "Etched and regrown vertical GaN junction barrier Schottky diodes," in *Proc. IEEE 8th Workshop Wide Bandgap Power Devices Appl. (WiPDA)*, Redondo Beach, CA, USA, Nov. 2021, pp. 288–292, doi: 10.1109/WiPDA49284.2021.9645135.

[11] J. Liu et al., "1.2-kV vertical GaN fin-JFETs: High-temperature characteristics and avalanche capability," *IEEE Trans. Electron Devices*, vol. 68, no. 4, pp. 2025–2032, Apr. 2021, doi: 10.1109/TED.2021.3059192.

[12] S. Kotzea, A. Debald, M. Heuken, H. Kalisch, and A. Vescan, "Demonstration of a GaN-based vertical-channel JFET fabricated by selective-area regrowth," *IEEE Trans. Electron Devices*, vol. 65, no. 12, pp. 5329–5336, Dec. 2018, doi: 10.1109/TED.2018.2875534.

[13] C. Yang et al., "GaN vertical-channel junction field-effect transistors with regrown p-GaN by MOCVD," *IEEE Trans. Electron Devices*, vol. 67, no. 10, pp. 3972–3977, Oct. 2020, doi: 10.1109/TED.2020.3010183.

[14] T. J. Anderson et al., "Activation of Mg implanted in GaN by multicycle rapid thermal annealing," *Electron. Lett.*, vol. 50, no. 3, pp. 197–198, Jan. 2014.

[15] Y. Zhang et al., "Vertical GaN junction barrier Schottky rectifiers by selective ion implantation," *IEEE Electron Device Lett.*, vol. 38, no. 8, pp. 1097–1100, Aug. 2017, doi: 10.1109/LED.2017.2720689.

[16] V. Meyers et al., "p-type conductivity and damage recovery in implanted GaN annealed by rapid gyrotron microwave annealing," *J. Appl. Phys.*, vol. 128, no. 8, Aug. 2020, Art. no. 085701, doi: 10.1063/5.0016358.

[17] S. R. Aid, T. Uneme, N. Wakabayashi, K. Yamazaki, A. Uedono, and S. Matsumoto, "Carrier activation in Mg implanted GaN by short wavelength Nd:YAG laser thermal annealing," *Phys. Status Solidi A*, vol. 214, no. 10, Oct. 2017, doi: 10.1002/pssa.201700225.

[18] T. Niwa, T. Fujii, and T. Oka, "High carrier activation of Mg ion-implanted GaN by conventional rapid thermal annealing," *Appl. Phys. Exp.*, vol. 10, no. 9, Aug. 2017, Art. no. 091002, doi: 10.7567/apex.10.091002.

[19] H. W. Choi, M. A. Rana, S. J. Chua, T. Osipowicz, and J. S. Pan, "Surface analysis of GaN decomposition," *Semiconductor Sci. Technol.*, vol. 17, no. 12, pp. 1223–1225, Dec. 2002, doi: 10.1088/0268-1242/17/12/304.

[20] A. G. Jacobs et al., "Role of capping material and GaN polarity on Mg ion implantation activation," *Phys. Status Solidi A*, vol. 217, no. 7, Apr. 2020, Art. no. 1900789, doi: 10.1002/pssa.201900789.

[21] M. H. Breckenridge et al., "High Mg activation in implanted GaN by high temperature and ultrahigh pressure annealing," *Appl. Phys. Lett.*, vol. 118, no. 2, Jan. 2021, Art. no. 022101, doi: 10.1063/5.0038628.

[22] H. Sakurai et al., "Highly effective activation of Mg-implanted p-type GaN by ultra-high-pressure annealing," *Appl. Phys. Lett.*, vol. 115, no. 14, Sep. 2019, Art. no. 142104, doi: 10.1063/1.5116866.

[23] K. Hirukawa et al., "Isochronal annealing study of Mg-implanted p-type GaN activated by ultra-high-pressure annealing," *Appl. Phys. Exp.*, vol. 14, no. 5, Apr. 2021, Art. no. 056501, doi: 10.35848/1882-0786/abf4f3.

[24] K. Sumida et al., "Effect of annealing time and pressure on electrical activation and surface morphology of Mg-implanted GaN annealed at 1300 °C in ultra-high-pressure nitrogen ambient," *Appl. Phys. Exp.*, vol. 14, no. 12, Nov. 2021, Art. no. 121004, doi: 10.35848/1882-0786/ac39b0.

[25] D. Khachariya et al., "Vertical GaN junction barrier Schottky diodes with near-ideal performance using Mg implantation activated by ultra-high-pressure annealing," *Appl. Phys. Exp.*, vol. 15, no. 10, Oct. 2022, Art. no. 101004, doi: 10.35848/1882-0786/ac8f81.

[26] M. Matys, K. Kitagawa, T. Narita, T. Uesugi, J. Suda, and T. Kachi, "Mg-implanted vertical GaN junction barrier Schottky rectifiers with low on resistance, low turn-on voltage, and nearly ideal nondestructive breakdown voltage," *Appl. Phys. Lett.*, vol. 121, no. 20, Nov. 2022, Art. no. 03507, doi: 10.1063/5.0106321.

[27] S. Rathkanthiwar et al., "Point-defect management in homoepitaxially grown Si-doped GaN by MOCVD for vertical power devices," *Appl. Phys. Exp.*, vol. 15, no. 5, Apr. 2022, Art. no. 051003, doi: 10.35848/1882-0786/ac6566.

[28] S. R. Stein et al., "Schottky contacts on ultra-high-pressure-annealed GaN with high rectification ratio and near-unity ideality factor," *Appl. Phys. Exp.*, vol. 16, no. 3, Mar. 2023, Art. no. 031006, doi: 10.35848/1882-0786/acc443.

[29] T. Narita, H. Sakurai, M. Bockowski, K. Kataoka, J. Suda, and T. Kachi, "Electric-field-induced simultaneous diffusion of Mg and H in Mg-doped GaN prepared using ultra-high-pressure annealing," *Appl. Phys. Exp.*, vol. 12, no. 11, Nov. 2019, Art. no. 111005, doi: 10.7567/1882-0786/ab4934.

[30] H. Sakurai et al., "Redistribution of Mg and H atoms in Mg-implanted GaN through ultra-high-pressure annealing," *Appl. Phys. Exp.*, vol. 13, no. 8, Jul. 2020, Art. no. 086501, doi: 10.35848/1882-0786/aba64b.

[31] B. J. Baliga, *Advanced Power Rectifier Concepts*. New York, NY, USA: Springer, 2009.

[32] A. M. Ozbek and B. J. Baliga, "Tunneling coefficient for GaN Schottky barrier diodes," *Solid-State Electron.*, vol. 62, no. 1, pp. 1–4, Aug. 2011, doi: 10.1016/j.sse.2011.04.016.

[33] I. C. Kizilyalli, A. P. Edwards, O. Aktas, T. Prunty, and D. Bour, "Vertical power p-n diodes based on bulk GaN," *IEEE Trans. Electron Devices*, vol. 62, no. 2, pp. 414–422, Feb. 2015, doi: 10.1109/TED.2014.2360861.

[34] Y. B. Acharya, "Effect of temperature dependence of band gap and device constant on I–V characteristics of junction diode," *Solid-State Electron.*, vol. 45, no. 7, pp. 1115–1119, Jul. 2001, doi: 10.1016/S0038-1101(01)00139-3.

[35] T. Mori et al., "Schottky barriers and contact resistances on p-type GaN," *Appl. Phys. Lett.*, vol. 69, no. 23, pp. 3537–3539, Dec. 1996, doi: 10.1063/1.117237.